https://doi.org/10.5194/egusphere-2026-2700
Preprint. Discussion started: 3 June 2026

A synoptic perspective on the role of the upstream diabatic cooling in modulating the North Pacific storm track

Franziska Schnyder[1] and Jacopo Riboldi[1]

[1]Institute for Atmospheric and Climate Science, ETH Zurich, Zurich, Switzerland

Correspondence: Franziska Schnyder (franziska.schnyder@usys.ethz.ch)

Abstract. Cold air outbreaks (CAOs) are an important driver of near-surface baroclinicity at the entrance of the northern hemispheric storm tracks during boreal winter. They originate over the upstream continent in regions of surface radiative cooling, suggesting that this diabatic process is not only important for CAO formation, but potentially also a relevant contributor to downstream storm track variability. Here, we aim to provide mechanistic insights into the underexplored link between upstream diabatic cooling and storm track variability in the context of CAOs. For this purpose, we analyze and compare distinct subsets of CAOs, characterized by stronger and weaker diabatic cooling over Siberia, occurring over the Japan Sea in the 1979-2023 period. To investigate the potential role of upstream diabatic cooling on storm track activity after CAOs, we quantify modulations of Eady growth rate (EGR) in the western North Pacific. In addition, we quantify the impact of diabatic cooling on the Siberian High, a semi-permanent weather system that has previously been associated with the occurrence of strong CAOs at the entrance of the North Pacific storm track.

With regards to low-level baroclinicity, we find that CAOs featuring enhanced upstream cooling are characterized by anomalously high EGR along the eastern coast of Russia and China. Further, peaks in EGR at the entrance of the storm tracks during winters between 1979-2023 are preceded by efficient radiative cooling over the continent, therefore contributing to a large temperature contrast between land and ocean. The contribution of diabatic processes to the intensification of the Siberian High is evaluated using the-sea level pressure (SLP) tendency equation. The diabatically driven SLP tendency at the time of maximum intensification amounts on average to 3.4 hPa $(6\,\mathrm{h})^{-1}$, and is of the same order of magnitude as the adiabatic contribution by horizontal and vertical motion. We also provide evidence that the land-based diabatic cooling indirectly supports, through baroclinic interaction, the amplification of an upper-level ridge-trough couplet that propagates into the storm tracks. The increased low-level baroclinicity and the deep upper-level trough at the entrance of the storm tracks, both enhanced by the upstream diabatic cooling, facilitate cyclogenesis at the entrance of the storm track. The resulting cyclones are more likely to be particularly deep, "bomb" cyclones and are associated with cyclonic wave breaking at upper-levels over the western North Pacific. On the other hand, we find no significant change in the number of cyclones developing in the 1-4 days following these CAO events: those subsequent cyclones remain small in size and do not exhibit strong intensification rates compared to climatology. In conclusion, our findings suggest that diabatic cooling over land takes an active role in shaping storm track variability, allowing us to mechanistically link upstream land–atmosphere thermodynamic processes to downstream extratropical cyclone activity.

https://doi.org/10.5194/egusphere-2026-2700
Preprint. Discussion started: 3 June 2026

1 Introduction

In the Northern Hemisphere the two main storm track regions are located in the North Pacific and North Atlantic (Hoskins and Hodges, 2002; Wernli and Schwierz, 2006), where baroclinicity is high due to the large land-sea contrast. Understanding storm track variability is especially important for weather forecasting as individual cyclones but also the frequent succession of individual cyclones, commonly referred to as cyclone clustering, may prompt extreme weather at the end of the storm tracks (e.g., Pfahl and Wernli, 2012; Pinto et al., 2014; Owen et al., 2021; Weijenborg and Spengler, 2026). Furthermore, the quest of drivers of storm track variability is also fueled by the desire of gaining sub-seasonal predictability in the extratropics, and of identifying dynamical constraints to disentangle contrasting climate projections of the extratropical circulations in a warmer climate.

Several studies have argued for the relevance of land-sea contrast in modulating the downstream storm tracks (e.g. Brayshaw et al., 2009; Portal et al., 2022, 2023). The oscillator model proposed by Ambaum and Novak (2014) and Novak et al. (2015) is a simple model relating storm track variability to the availability of baroclinicity. According to this theory, the jet stream, and with it the storm tracks, shifts in latitude based on fluctuations in baroclinicity at the entrance of the storm tracks. In that framework, baroclinicity is slowly but constantly replenished by a source term representing upstream diabatic cooling. However, neither the oscillator model nor other studies that focused on land-sea contrast studies provided detailed insights into which processes determine the availability of baroclinicity at the entrance of the storm tracks.

Recent studies argue that cold air outbreaks (CAOs) occurring at the entrance of the storm tracks, as well as latent heat release from intensifying cyclones are responsible for replenishing near-surface and mid-tropospheric baroclinicity in the storm track regions (Papritz and Spengler, 2015; Vannière et al., 2017; Marcheggiani et al., 2025; Marcheggiani and Spengler, 2025). Aside from influencing near-surface baroclinicity at the entrance of the storm tracks, CAOs have also been suggested to facilitate environments conducive to explosive cyclogenesis (Kuo et al., 1991; Bosart, 1981; Gyakum and Danielson, 2000). Less is known about the relevance of diabatic cooling over the upstream continent in contributing to the baroclinicity at the entrance of the storm tracks. A sensitivity study by Portal et al. (2023) showed that the presence of a cold anomaly in central Asia provides a stationary forcing for planetary-scale waves in the storm track regions. Furthermore, Schnyder and Riboldi (2026) showed that diabatic cooling over the upstream continents is crucial for determining the intensity of CAOs occurring at the entrance of the storm tracks, and the turbulent heat fluxes associated with them. These studies provide first indications that also diabatic cooling over the upstream continents are relevant contributors to the maintenance and amplification of baroclinicity at the entrance of the storm tracks.

Strong CAOs in the Japan Sea are linked to the presence of a strong Siberian High upstream, indicative of an amplified flow at upper-levels (Shoji et al., 2014; Schnyder and Riboldi, 2026). Takaya and Nakamura (2005b) find that that periods of amplified Siberian Highs co-occur with Ural Blocking and therefore argue that the intensification of the Siberian High is a result of baroclinic interaction with an upper-level ridge. On the other hand, diabatic cooling in central Siberia is also linked to the formation of the semi-permanent Siberian High (e.g., Wexler, 1951; Curry, 1987). Persistent land-based radiative cooling during the winter months at high latitudes promotes anticyclogenesis, whereby cooling-induced near-surface thickness

https://doi.org/10.5194/egusphere-2026-2700
Preprint. Discussion started: 3 June 2026

change is balanced by mid-level convergence (Wexler, 1937; Ding and Krishnamurti, 1987). Schnyder and Riboldi (2026) find that CAOs in the Japan Sea characterized by enhanced upstream diabatic cooling are preceded by the development of a strong surface anticyclone in central Siberia. They argue that both diabatic cooling and interaction with an upper-level ridge are important for the formation of this anticyclone albeit without quantifying the individual contributions explicitly. This suggests another mechanism through which diabatic cooling prior to CAOs affects the North Pacific storm track: by diabatically contributing to the Siberian High and the amplified flow at upper levels. Again, the mechanisms behind this link are yet to be explored in detail.

In this study, we shed light onto the role of upstream land-based diabatic cooling for North Pacific storm track activity and characteristics through the mechanism of baroclinicity modulation and Siberian High amplification in the context of CAOs. We do so by building on the categorization of CAOs occurring in the Japan Sea into large and small contributions from the upstream *boreal cold air reservoir* (C_{BCAR}), which was introduced in Schnyder and Riboldi (2026) and that can be regarded as indicative of periods of stronger and weaker diabatic cooling influence on the North Pacific storm track. In Section 3, we present differences in low-level baroclinicity, in the periods prior to and after large and small C_{BCAR} CAOs. The diabatic contribution to the Siberian High and potential interaction with the upper-level wave train is explored in Section 4. We then investigate how differences in baroclinicity and the upper-level wave impact cyclone number and characteristics during the period of the CAOs featuring large and small C_{BCAR} in Section 5, followed by a synthesis in Section 6.

2 Data and Methods

In this study we use the ERA5 reanalysis, provided by the European Center for Medium-Range Weather Forecasts (ECMWF), interpolated on a spatial grid of 0.5° x 0.5°, with 98 vertical hybrid sigma-pressure levels and a time resolution of 1 h (Hersbach et al., 2020). We consider time periods around 98 specific CAO events that have occurred within the winter months December, January, and February (DJF) between 1979–2023.

2.1 CAO events with strong or weak diabatic cooling

As a proxy for periods with strong and weak cooling over the land, we make use of previously identified CAO events in the Japan Sea, that are indicative of stronger or weaker cooling over the upstream land surface (Schnyder and Riboldi, 2026). These CAO events are selected based on particularly high values in the cold air outbreak index (CAOI) defined as $\theta_{SST} - \theta_{850}$ (Papritz et al., 2015) in the Japan Sea. Categorization of the CAO events is achieved based on Lagrangian trajectory analysis using the LAGRANTO tool Sprenger and Wernli (2015). Seven-day backward trajectories are initiated within the planetary boundary layer of the CAO events: those trajectories, which experience substantial diabatic cooling near the land surface, are identified as so-called BCAR trajectories (where p $>$ 700 hPa during the 7 days, the trajectories remain above the land surface and exhibit θ<280 K for at least 3 days, and are collocated with an anticyclone at least once). For each CAO event, the BCAR contribution (C_{BCAR}) to a given CAO event is evaluated as a proxy for how strongly diabatic cooling over the upstream continent affects the CAO events.

https://doi.org/10.5194/egusphere-2026-2700
Preprint. Discussion started: 3 June 2026

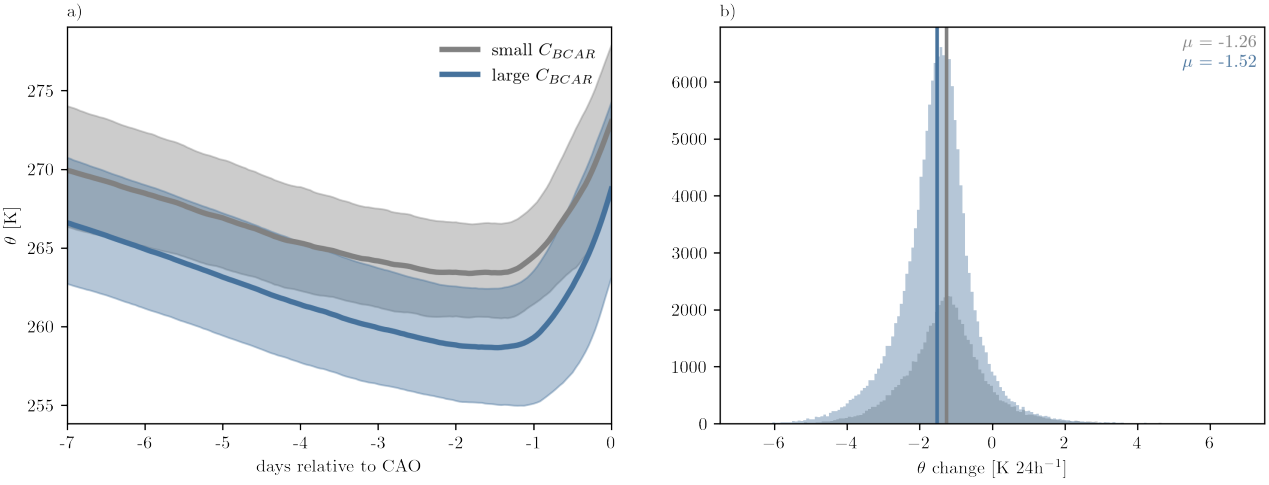

Figure 1. Composite of 7-day backward trajectory analysis of CAO events in the Japan Sea featuring large and small C_{BCAR} (49 events each). In a) the mean evolution of BCAR trajectories is indicated with solid lines and the interquartile range in shading. The distribution of the 24 h diabatic cooling rates along the BCAR trajectories between $t_{CAO} - 6\,d$ and $t_{CAO} - 2\,d$ are additionally shown in b).

$$C_{BCAR} = \underbrace{\frac{N_{BCAR}}{N_{total}}}_{\text{(a)}} \cdot \underbrace{\left(1 - \frac{\theta_{BCAR} - \theta_{BCAR,coldest}}{\theta_{BCAR,warmest} - \theta_{BCAR,coldest}}\right)}_{\text{(b)}}, \tag{1}$$

where N_{BCAR} denotes the number of BCAR trajectories, N_{total} the total number of CAO trajectories associated with the event, and θ_{BCAR} is the mean of the lowest θ values reached along each BCAR trajectory. The minimum ($\theta_{BCAR,coldest}$) and maximum ($\theta_{BCAR,coldest}$) values of θ_{BCAR} among all CAO events are identified, to obtain an event relative ranking. Consequently, C_{BCAR} assumes values between 0 and 1. C_{BCAR} is large when a large share of trajectories involved in a given CAO event are identified as BCAR trajectories and their minimum θ is comparatively low. Based on C_{BCAR}, we obtain 2 subsets of CAO events, featuring small and large C_{BCAR} (both groups constituting 49 events each). For more information on the exact event determination and categorization see Schnyder and Riboldi (2026).

The average θ evolution up to the CAOs maximum intensity (defined as the time with the highest CAOI; t_{CAO}), as well as the 24 h cooling rates of BCAR trajectories involved in the two types of events show that trajectories cool more strongly prior to CAOs featuring large C_{BCAR} (Fig. 1). The differences in cooling rates, as well as the constraint that BCAR trajectories must spend at least 3 consecutive days over land surface, can be taken as indication that prior to large C_{BCAR} CAOs land based cooling over the upstream continent is enhanced compared to small C_{BCAR} CAOs. Note that the difference in the number of trajectories arises by design of C_{BCAR}.

https://doi.org/10.5194/egusphere-2026-2700
Preprint. Discussion started: 3 June 2026

2.2 Diagnostics: Eady growth rate, net radiation, and quasi-geostrophic forcing for ascent

Net radiation. Daily mean net radiation at the surface offers insights into the contribution of radiation to surface heating. It is calculated as the algebraic sum in incoming and outgoing shortwave and longwave radiation at the surface, whereby negative values indicate more outgoing than incoming radiation (i.e., net energy loss at the surface). Daily averages are computed using 3-hourly ERA5 data. As we focus here on mid- and high latitudes during winter, net radiation will be particularly modulated by the strength of surface longwave cooling.

Eady growth rate. Baroclinicity is quantified using the Eady growth rate (EGR) calculated following Besson et al. (2021). EGR at 700 hPa is evaluated as a function of static stability and the vertical shear of the horizontal wind between 500 and 850 hPa as the upper and lower bound (for more information see Besson et al., 2021).

Quasi-geostrophic forcing for ascent. Quasi-geostrophic forcing for ascent and descent (QGω) is calculated as in Davies (2015) from the inverted QGω equation in its Q-vector formulation. Here, we evaluate QGω at 600 hPa forced by the Q-vector divergence computed at upper levels (i.e., all levels below 550 hPa; for more detailed information see Besson et al., 2021). This variable can provide useful information on the strength of the upper-level trough associated with the growth of cyclones that initiate the CAOs.

Statistical significance assessment. Anomalies are obtained with respect to a daily mean that is corrected for the seasonal cycle and climate change trends using a 21-day and 9-year running window. Statistical significance of the anomalies are evaluated with a bootstrapping approach featuring 1000 repetitions. The relevant p-values for the significant assessments are determined using the false discovery rate following Wilks (2016).

2.3 Anticyclone tracking

As we are particularly interested in quantifying the contribution of diabatic processes to the anticyclones that develop over Siberia preceding large C_{BCAR} CAOs, we identify and track surface anticyclones as local maxima in the sea-level pressure (SLP) field. The outermost contour enclosing the SLP maxima (while not exceeding a maximum length of 15'000 km) is then searched iteratively by the algorithm, yielding a 2-dimensional anticyclone mask. The subsequent anticyclone tracking then constructs a plausible anticyclone track by connecting the position of anticyclone centers in time, using a first guess of anticyclone motion based on recent propagation and suitable threshold criteria. For more details about the tracking, see (Sprenger et al., 2017, their supplement). Since anticyclone centers are generally less well-defined as cyclone centers (especially over land) we do not track all local SLP maxima, as this may result in up to 20-30 tracked centers per anticyclone mask. Instead, we identify the maximum SLP for each anticyclone mask at a 6 h time resolution, and track only these maxima. The relevant anticyclones were then chosen individually by inspecting all anticyclone tracks in the periods between $t_{CAO} - 10$d and $t_{CAO} - 0$d. For each event, we aim to find the most intense anticyclone in terms of SLP in central Siberia, that contributes to the anticyclonic anomaly in the SLP composite (see Fig. 10 in Schnyder and Riboldi, 2026). Cyclone tracking and anticyclone tracking over land based on SLP fields is difficult, since SLP over land are (locally strongly) extrapolated, leading to "jumpy" and unphysical tracks at times. By individually selecting the anticyclones, we avoid selecting such anticyclones. The procedure

https://doi.org/10.5194/egusphere-2026-2700
Preprint. Discussion started: 3 June 2026

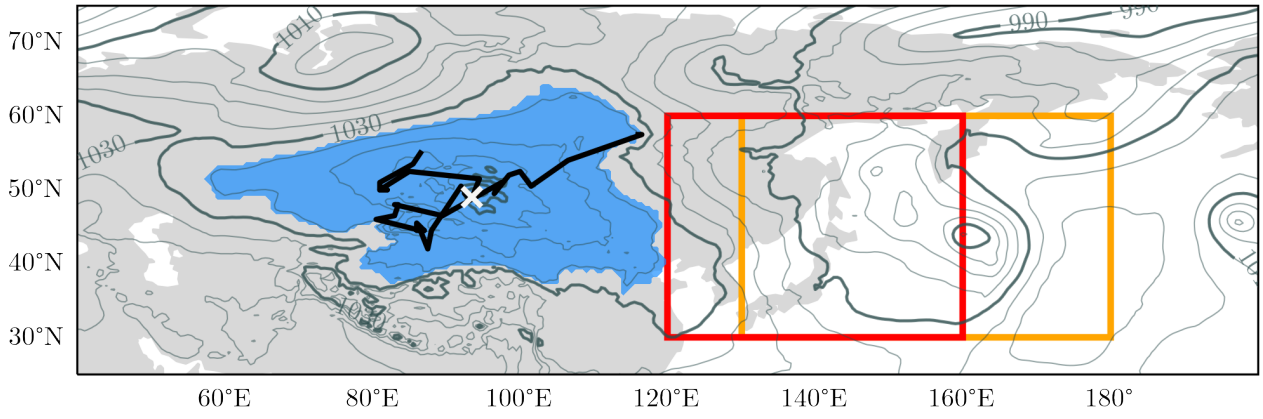

Figure 2. Example of a selected anticyclone track with maximum intensification on 00 UTC on 30 January 1996. The anticyclone mask is shown in blue shading and the track in the black line, with the location of the maximum intensification indicated by a white cross. SLP at the time of the anticyclone's maximum intensification is shown in gray contours (every 5 hPa). We additionally show the boxes used for the identification of primary cyclones that initiate the CAOs (red) and subsequent cyclones that develop after the CAOs (orange; see Sect. 2.5).

leads to a selection of 42 anticyclones over the 49 considered CAO events with high C_{BCAR}. For 7 out of the 49 considered events, it was not possible to identify an anticyclone in central Siberia.

2.4 Quantification of diabatic contribution to anticyclone intensification with the SLP tendency equation

For the quantification of the role of diabatic processes for the intensification of our selected anticyclones, we make use of the SLP tendency equation derived by Fink et al. (2012). The SLP tendency equation quantifies the contributions of different processes as follows:

$$\frac{\partial p_{sfc}}{\partial t} = \underbrace{\rho_{sfc}\frac{\partial \phi_{p_2}}{\partial t}}_{D\phi} + \underbrace{\rho_{sfc} R_d \int_{sfc}^{p_2} \frac{\partial T_v}{\partial t} d\ln p}_{ITT} + \underbrace{g(E-P)}_{EP} + RES_{PTE}, \tag{2}$$

where p_{sfc} denotes the surface pressure, ρ_{sfc} the air density at the surface, ϕ_{p_2} the geopotential at p_2, R_d the gas constant for dry air, T_v the virtual temperature, g the gravitational acceleration, E the evaporation, and P precipitation. Following the equation the surface pressure may change as a function of the change in geopotential at the column top ($D\phi$), changes in the temperature profile (ITT), and mass variation due to evaporation and precipitation of water (EP). RES_{PTE} quantifies the residual changes that are otherwise unaccounted for.

The temperature-related tendency ITT may be further expanded to separate contributions of different physical processes to SLP change:

https://doi.org/10.5194/egusphere-2026-2700
Preprint. Discussion started: 3 June 2026

$$ITT = \underbrace{\rho_{sfc} R_d \int_{sfc}^{p_2} -\mathbf{v} \cdot \nabla_p T_v d\ln p}_{ADV} + \underbrace{\rho_{sfc} R_d \int_{sfc}^{p_2} \left(\frac{R_d T_v}{c_p p} - \frac{\partial T_v}{\partial p} \right) \omega d\ln p}_{VMT} + \underbrace{\rho_{sfc} R_d \int_{sfc}^{p_2} \frac{T_v Q}{c_p T} d\ln p}_{DIAB} + RES_{ITT}, \quad (3)$$

where $\mathbf{v}$ and ω are the horizontal and vertical wind components, T is temperature, c_p the specific heat capacity at constant pressure, and Q the diabatic heating rate. Isobaric temperature advection (ADV) and vertical motion (VMT) describe the adiabatic column integrated temperature tendency, whereas $DIAB$ accounts for column integrated temperature tendencies due to diabatic processes, such as radiation, latent heating, and mixing due to turbulence. RES_{ITT} describes the error for budget closure. Equation 1 and 2 are calculated based on the 6 h SLP changes. For the calculation of $DIAB$ we use the hourly mean temperature tendencies due to the physical parameterizations from ERA5. We evaluate the terms contributing to the anticyclone's intensification by averaging around the anticyclone centers in a 500 km radius at the time of the anticyclone's maximum intensification (defined as maximum 6 h SLP increase).

2.5 Cyclone tracks and identification of cyclones developing before and after the CAOs

To investigate the reaction of the storm tracks to large and small C_{BCAR} CAOs, we use the cyclone track dataset by Wernli and Schwierz (2006) and refined by Sprenger et al. (2017). The cyclones are identified as local minima in SLP field and tracked with the same tracking algorithm as the anticyclones.

We identify the cyclones responsible for the CAO initiation (primary cyclones), by considering the cyclones located in the CAO region (approximated with a second box spanning (120° - 160°E and 30° - 60°N) in the 24 hours preceding the CAO's maximum intensity (Fig. 2). The deepest, still intensifying (i.e., Bergeron unit > 0) cyclone in that region, is considered the "primary" cyclone. The tracks of the selected cyclones are shown in the supplement (Fig. S4). Evaluation of maximum intensification rates (defined using the 24 h pressure drop, i.e., in Bergeron units), and maximum depth allows for comparison of the primary cyclones associated with large or small C_{BCAR} CAOs as well as primary and subsequent cyclones.

The additionally count the number of cyclones and explosively deepening cyclones featuring intensification rates higher than 24 hPa (24 h^{-1}), i.e., one Bergeron unit, after the occurrence of the CAOs is counted in a box covering the western portion of the North Pacific storm track (130° - 180°E and 30° - 60°N; Fig. 2). This is done for several aggregation periods: 1 - 2 days, 1 - 3 days and 1 - 4 days after the CAOs maximum intensity, whereby maximum intensification must occur within the box within the given time period in order for the cyclone to count. Note that we start only 1 day after the CAO's maximum intensity in order to avoid counting the cyclone initiating the CAOs themselves.

https://doi.org/10.5194/egusphere-2026-2700
Preprint. Discussion started: 3 June 2026

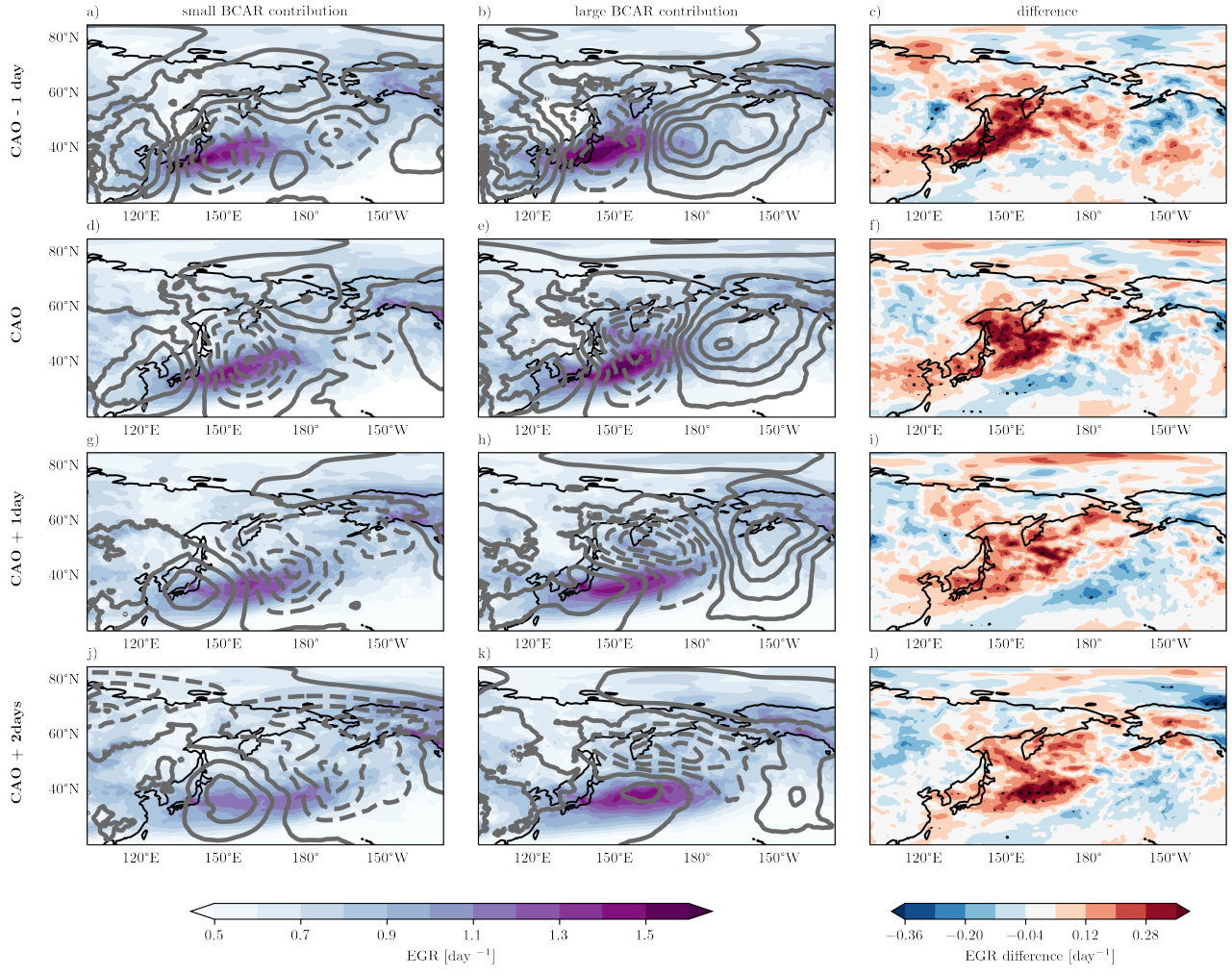

Figure 3. Composite of EGR at 700 hPa (shading) and SLP anomalies (gray contours) at (a, b) $t_{CAO} - 1$d, (c, d) t_{CAO}, (e, f) $t_{CAO} + 1$d, (g, h) $t_{CAO} + 2$d for CAO featuring small BCAR contributions (left) and large BCAR contributions (right). The difference between the two categories (large − small BCAR contributions) are indicated in the right panel (c,f,i,l).

3 Results

3.1 The role of the upstream diabatic cooling in enhancing baroclinicity at the entrance of the storm tracks

We first examine the evolution of EGR during CAO events with large and small C_{BCAR} to elucidate the role of diabatic cooling in providing baroclinicity at the entrance of the North Pacific storm track.

The days leading up to CAOs are almost by definition characterized by particularly high baroclinicity, as large amounts of cold air are stored over the continent waiting to be released towards the ocean (Schnyder and Riboldi, 2026). Accordingly,

https://doi.org/10.5194/egusphere-2026-2700
Preprint. Discussion started: 3 June 2026

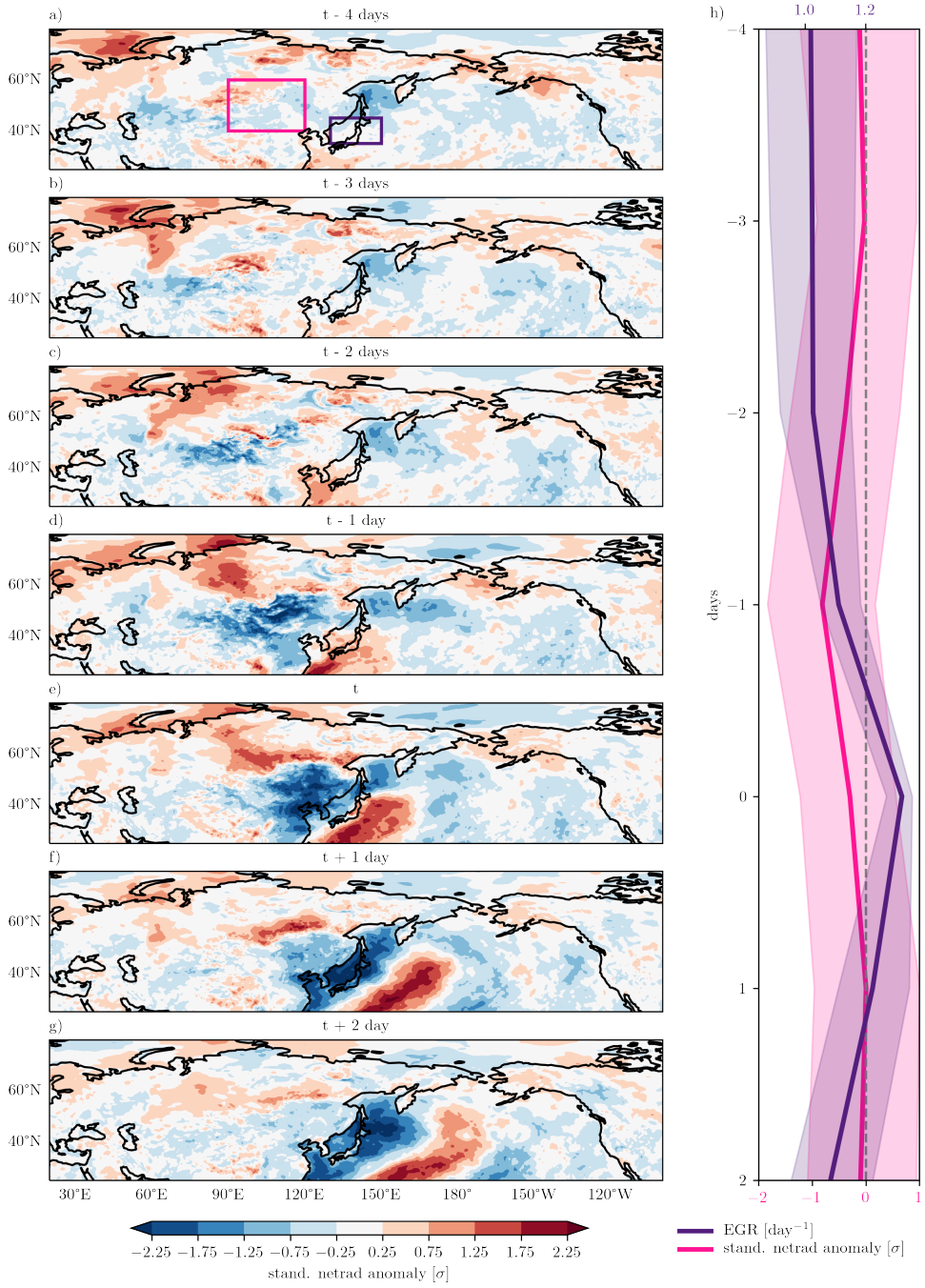

Figure 4. Composite of standardized net radiation anomalies relative to time steps when the box averaged daily EGR at 700 hPa exceed the 90th percentile (237 events in DJF between 1979-2023) at (a) $t-4$d, (b) $t-3$d, (c) $t-2$d, d) $t-1$d, (e) t, (f) $t+1$d, and (g) $t+2$d. On the right (h), we show a time series of box averaged EGR and standardized net radiation anomaly over the same time period. The solid line indicates the mean, and the shading the interquartile range. The box used to obtain the EGR time series is shown in purple, and the one for the standardized net radiation anomaly in pink.

https://doi.org/10.5194/egusphere-2026-2700
Preprint. Discussion started: 3 June 2026

we find high EGR along the Asian coast line and over Japan shortly before the time of strong CAOs (Fig. 3a,b). Moreover, EGR along the coast line prior to large C_{BCAR} CAOs are higher than prior to small C_{BCAR} CAOs (Fig. 3c). Compared to a daily climatology, EGR anomalies along the coast line locally amount to $0.4\,\mathrm{day}^{-1}$ before large C_{BCAR} CAOs, as opposed to $0.2\,\mathrm{day}^{-1}$ before small C_{BCAR} CAOs (see Fig. S1 in the supplement). Given climatological values of roughly $1.0\,\mathrm{day}^{-1}$ during the winter months in the same region, anomalies of such magnitude indicate substantial local increases in the EGR.

After the CAO, at $t_{CAO} + 1\mathrm{d}$, the baroclinic zone is shifted further away from the coast and into the storm track region compared to the days before (Fig. 3a,b,g,h). In the case of large C_{BCAR} CAOs, this shift results from the primary cyclone remaining fairly stationary in the vicinity of Kamchatka, allowing persistent advection of cold air from the continent towards the North Pacific (Fig. 3h,k). The slow movement of the cyclone is likely linked to the stationary character of the upper level trough, whose eastward propagation is hindered by the establishment of a blocking ridge over the Eastern North Pacific (see Sect. 3.3), as well as the large and deep nature of the primary cyclones themselves. Comparing the two categories, we find that the baroclinic zone after large C_{BCAR} CAOs is still larger than the one after small C_{BCAR} CAOs (Fig. 3j,k). This difference in remaining baroclinicity may be due to differences in the location of the primary cyclone (note how the primary cyclone associated with small C_{BCAR} CAOs tracks more eastward than poleward), or to stronger latent heating in the primary cyclone associated with large C_{BCAR} CAOs, replenishing baroclinicity in the wake of the cyclone (Marcheggiani and Spengler, 2023; Marcheggiani et al., 2025).

The composite analysis centered on CAO events suggests that baroclinicity at the entrance of the storm tracks oscillates as a function of upstream radiative cooling and the cyclones within the storm tracks. To further investigate this hypothesis, we additionally analyze events of particularly high area-averaged EGR along the east Asian coast (130°-150°E and 35°-40°N, see Fig. 3). Considering all events in which the box-averaged, daily mean EGR exceeds the 90th percentile leads to the identification of 237 events (in DJF between 1979-2023).

Indeed, composites and box averaged time series centered on baroclinicity peaks are preceded by efficient near-surface radiative cooling over the upstream land surface, denoted by negative anomalies in net radiation (Fig. 4). Approximately 2 days before the onset time steps, first signs of negative net radiation anomalies appear in central Siberia (Fig. 4c,h). In these regions, where net radiation is already climatologically negative, energy loss at the surface is unusually high due to clear sky conditions and thus indicates more efficient surface radiative cooling (also reflected in negative total column water anomalies in Fig. S2 in the supplement). During the following 2 days negative net radiation anomalies increase with up to 2σ in northern China, the Korean Peninsula and along the Russian coast (Fig. 4d,e,h). The surface based cooling locally tilts the isentropes over land, increasing the EGR near the coastline, which peaks on the day of 90th percentile exceedance (Fig. 4h). Strong positive anomalies southeast of Japan, on the other hand, indicate particularly cloudy conditions likely related to the formation of a cyclone: there, solar incoming radiation at the surface is reduced and incoming longwave radiation is increased. The two would then sum up to a net positive energy flux at the surface. Finally, the EGR in the Japan Sea decreases as the high baroclinicity is consumed by the developing cyclone and upstream radiative cooling weakens (Fig. 4f,g,h). At these times negative net radiation anomalies prevail in the Japan Sea, suggesting an overall reduced tropospheric water load likely associated with the occurrence of a CAO (Fig. 4f,g).

https://doi.org/10.5194/egusphere-2026-2700
Preprint. Discussion started: 3 June 2026

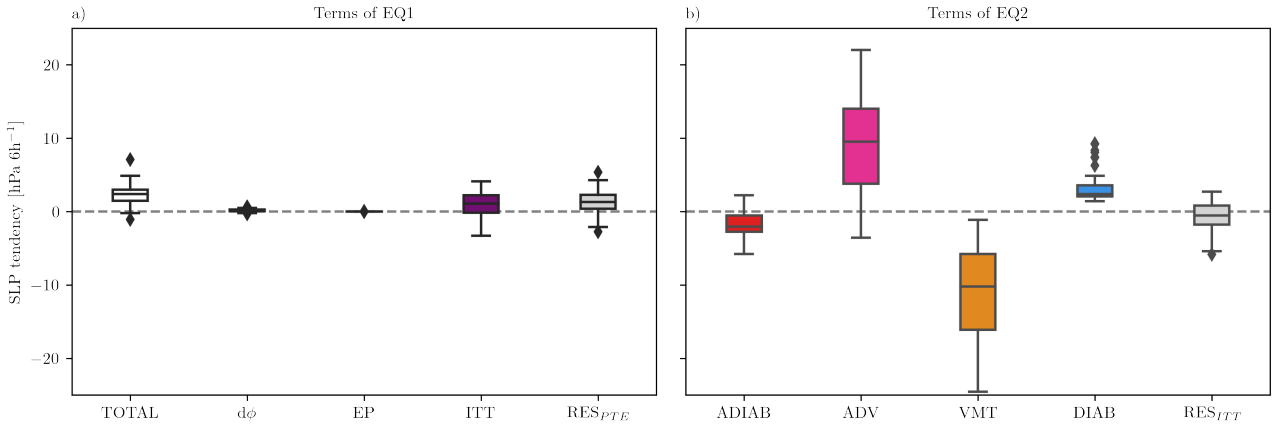

Figure 5. Processes contributing to changes in the SLP, evaluated around 42 anticyclone centers (r = 500 km) at the time of their maximum intensification.

In summary, the correspondence between low-level baroclinicity at the entrance of the North Pacific storm track and upstream net radiation anomalies is not only limited to CAO events. While our findings generally agree with the fact that cyclones are important for the evolution of baroclinicity inside storm track regions (e.g., Papritz and Spengler, 2015; Marcheggiani and Spengler, 2023), they also highlight the role of upstream diabatic cooling in replenishing low-level baroclinicity at the entrance of the storm tracks, (as postulated by, e.g., Namias, 1950; Ambaum and Novak, 2014).

3.2 Diabatic amplification of the Siberian High estimated from the SLP tendency equation

In addition to contributing to high EGR at the entrance of the storm tracks, radiative cooling has been suggested to contribute to the formation of a strong Siberian High (Wexler, 1951), thus exerting an indirect influence on the downstream storm tracks via processes such as the modulation of low-level cold air advection.

Quantification of the diabatic contribution to the surface anticyclone's intensification is achieved using the SLP tendency equation derived by Fink et al. (2012). Indeed, we find that at the time of the anticyclones' maximum intensification, diabatic processes contributes to an average pressure increase of about 3.4 hPa (6 h^{-1}) in correspondence to the anticyclone's center (DIAB; Fig. 5b). The adiabatic processes contributing to changes in the vertical temperature profile, and thus in pressure in the center of the anticyclone, include temperature advection (ADV) and vertical motion (VMT): individually, their contributions are large in magnitude (Fig. 5b), but their opposite tendencies largely compensate each other (cold air advection being balanced by subsidence), leading to an overall small and even slightly negative adiabatic contribution (ADIAB) to the SLP change. The cancellation of the two adiabatic terms emphasizes the importance of diabatic cooling for the surface anticyclones upstream of CAOs, as the order of magnitude of ADIAB is comparable to the one of DIAB. In comparison to the large contributions of the diabatic and adiabatic terms to ITT, contributions from $D\phi$ are very small, which indicates no change in the total column

https://doi.org/10.5194/egusphere-2026-2700
Preprint. Discussion started: 3 June 2026

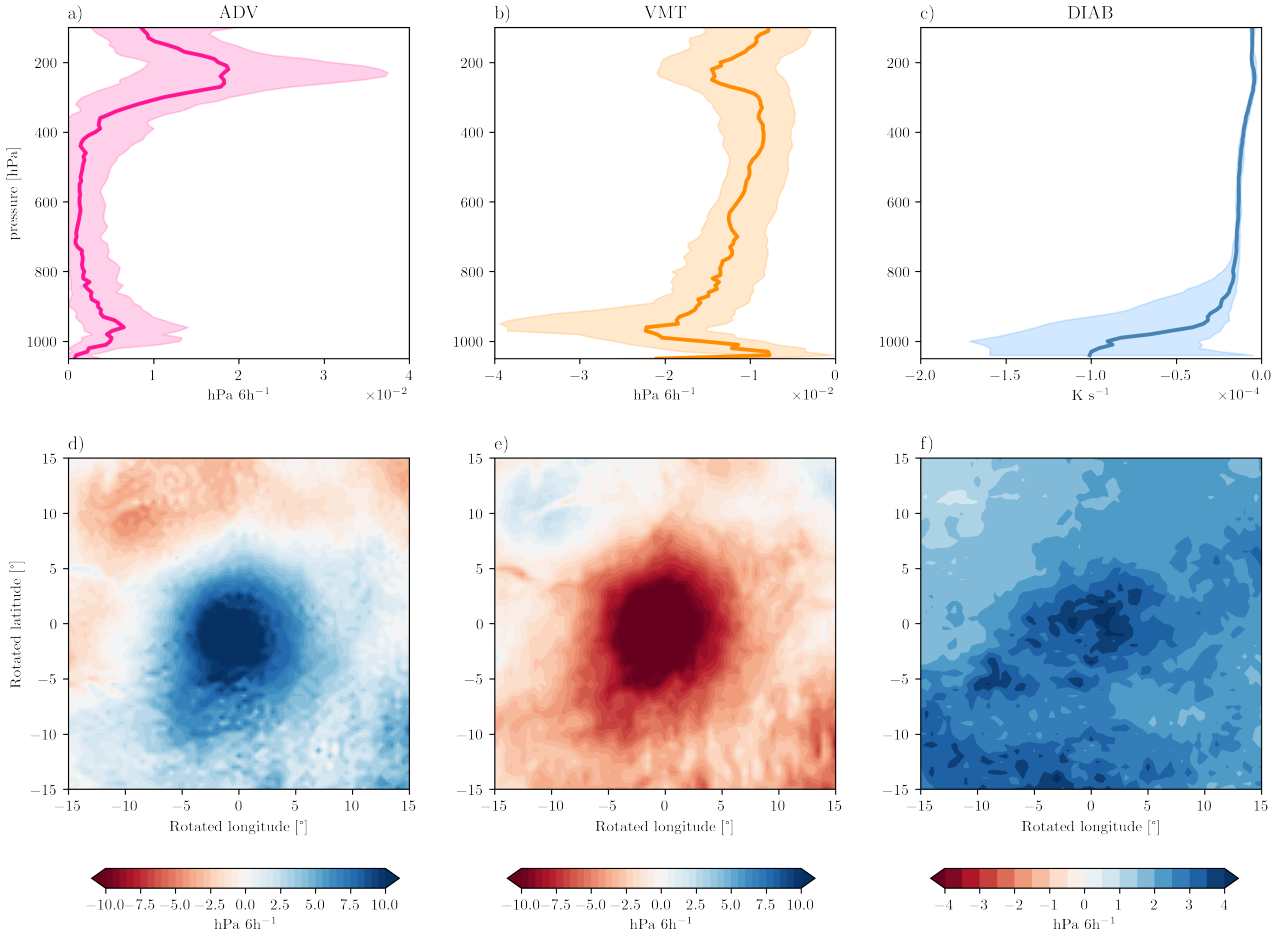

Figure 6. Composites of the processes contributing to ITT at the time of the anticyclones' maximum intensification as separated in 3: (a,d) the temperature advection term, (b,e) the vertical motion term, and (c,f) the diabatic term. The top row (a-c) shows the vertical profile averaged in a 500 km radius around the anticyclones' center. The bottom row (d-f) shows the anticyclone centered, horizontal cross section of the column integral.

height considered (Fig. 5a). The EP term is also negligible, reflecting the very dry environment found over Siberia during winter (Fig. 5a).

Anticyclone-centered composites (Fig. 6) provide more information on the horizontal and vertical structure of the physical processes associated with the SLP changes decomposed in Eq. 3. The temperature advection and vertical motion term both show clear contributions to SLP tendencies close to the anticyclone center (Fig. 6d,e). In terms of temperature advection, a clear peak is discernible at upper-levels, where wind speeds are large and cold air advection accordingly strong (Fig. 6a). In contrast, subsidence occurs throughout the entire column, with two distinct peaks at about 200 hPa and 950 hPa, likely related to peaks in upper-level convergence and vertical diabatic cooling gradient at these heights, respectively (Fig. 6b,c). The

https://doi.org/10.5194/egusphere-2026-2700
Preprint. Discussion started: 3 June 2026

composites further emphasize the previous observation that the vertical motion term acts to override the temperature advection term, as the magnitudes in SLP tendencies due to vertical motion are larger compared to those due to temperature advection in a radius of 5° around the anticyclone center – thus largely compensating each other and summing up to negative SLP tendencies. The deciding factor then lies in the diabatic term, which contributes to a SLP increase in the entire domain around the anticyclone, but shows enhanced tendencies in and around the anticyclone center (Fig. 6f). The vertical profile reveals the bottom-heavy structure of the diabatic contribution, further highlighting the importance of near-surface cooling for anticyclone deepening (Fig. 6c).

The closure of the total budget is problematic, as the residual of eq. 3 is non-negligible (Fig. 5). One possible explanation is that the diagnostic for SLP tendencies is applied to land regions, where SLP values are extrapolated in regions of complex terrain and high elevation. Given that the largest spread is found for the ADV and VMT terms, we believe that those terms are the most important contributors to the residual: this also reflects in the uncertainty in the sign of the ADIAB term. Nevertheless, the small spread in the diabatic term indicates a consistently positive contribution to the pressure tendency, supporting the hypothesis that diabatic cooling over the continent is an important contributor to the surface anticyclone's formation and depth. Furthermore, the diabatic pressure tendencies in this study are derived directly from the ERA5 diabatic temperature tendencies, and not diagnosed as residual of the ITT budget (as done in previous applications of the SLP budget diagnostic to ERA5 data, e.g., Qian et al., 2023; Christ et al., 2025). This contributes to an overall reduction in the uncertainty, and lends further support in our conclusions about the importance of diabatic processes in modulating the Siberian High intensity and, consequently, the downstream storm track activity.

3.3 Amplification of upper-level wave trains via baroclinic interaction with enhanced an Siberian High

It's no coincidence that diabatic cooling is efficient in the region of the intensifying surface anticyclone. Advection of dry air from the Arctic on the western side of the trough and the subsidence within the anticyclone favor clear-sky conditions, where long-wave radiative cooling from the land surface can efficiently cool the lower troposphere (see polar anticyclone in Wexler, 1951; Curry, 1983). Indeed composites of net radiation anomalies show negative anomalies on the southeastern edge of the eastward propagating Siberian anticyclone and underneath the upper-level trough prior to large C_{BCAR} CAOs, indicative of enhanced net energy loss at the surface (Fig. 7b,d,f). The days prior to small C_{BCAR} CAOs do not show similar signs of enhanced net radiative energy loss in the absence of a surface anticyclone (Fig. 7a,c,e). We conclude that the upper-level ridge/trough couplet itself provides favorable conditions for efficient diabatic cooling, which in turn intensify the low-level anticyclone again (as shown from the SLP tendency equation).

Takaya and Nakamura (2005a, b) showed that periods of particularly intense Siberian Highs coincide with periods of Ural blocking, and proposed that baroclinic interaction between the two can lead to further amplification of the surface Siberian High. In agreement with Takaya and Nakamura (2005a, b), composites of upper-level geopotential height anomalies indicate the presence of a distinct upper-level wave train prior to large C_{BCAR} CAOs, during the surface anticyclone's intensification. The development of this wave train starts from a ridge anomaly located over the Ural mountains at $t_{CAO} - 10\,d$ that persists thereby until $t_{CAO} - 4\,d$, a remarkable persistence likely indicative of a Ural blocking (not shown, Fig. 7b,d). From $t_{CAO} - 6\,d$

https://doi.org/10.5194/egusphere-2026-2700
Preprint. Discussion started: 3 June 2026

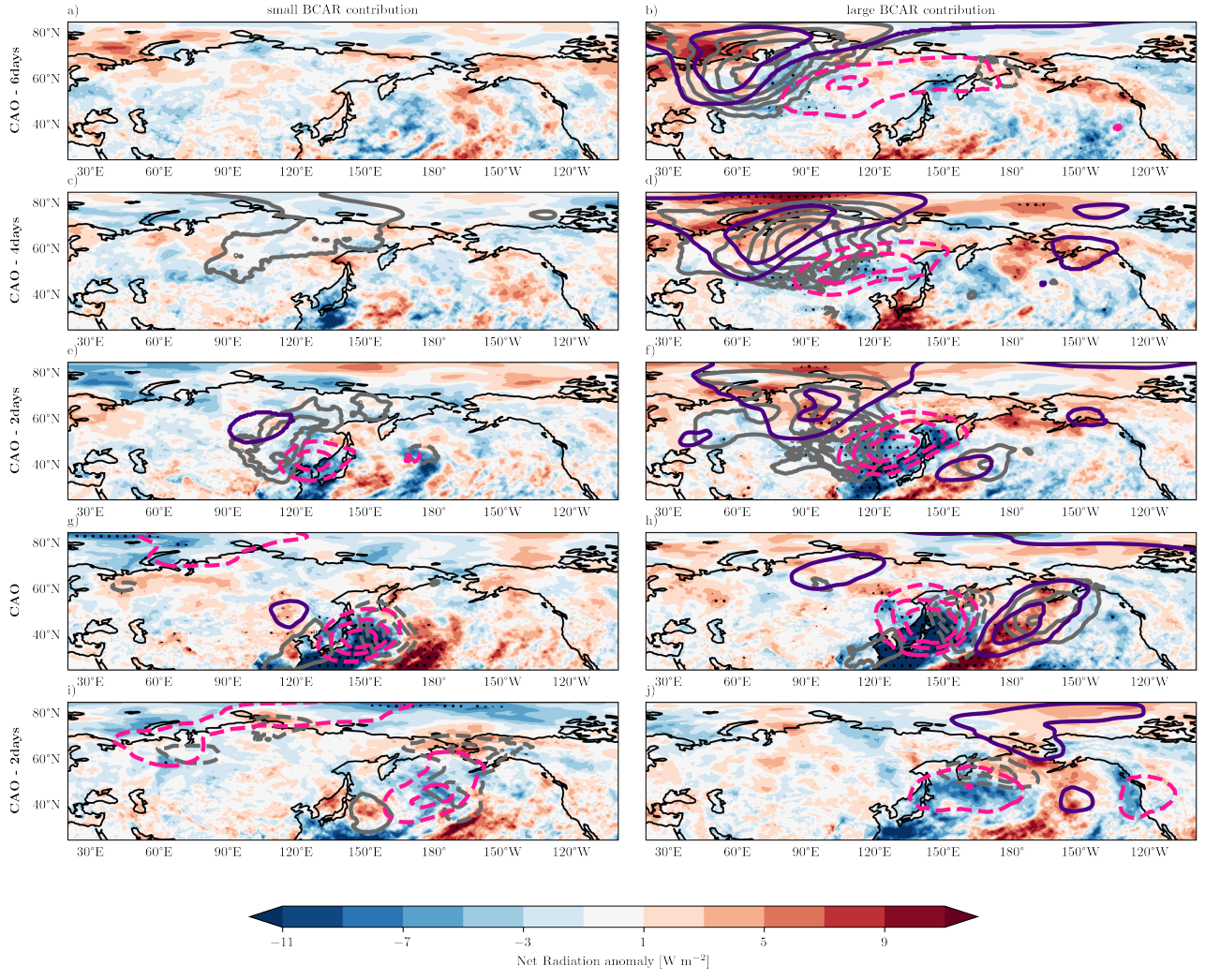

Figure 7. Composite of net radiation anomalies (shading), SLP anomalies (gray contours, dashed for negative and solid for positive), and geopotential height anomalies at 500 hPa (colored contours, pink for negative and blue for positive) at (a, b) $t_{CAO} - 5\,d$, (c, d) $t_{CAO} - 4\,d$, (e, f) $t_{CAO} - 3\,d$, (g, h) $t_{CAO} - 2\,d$, (i, j) t_{CAO}, and (k, l) $t_{CAO} + 2\,d$ for CAO featuring small BCAR contributions (left) and large BCAR contributions (right). Significant net radiation anomalies are indicated in stippling.

there are first signs of downstream development with the formation of a trough in East Asia (Fig. 7d). As the upper-level wave slowly propagates east in the following days, the trough intensifies and a new ridge anomaly develops over the North Pacific (Fig. 7d,f,h). However, propagation of the trough into the central North Pacific appears blocked by the growing ridge downstream, such that it remains stationary near Kamchatka from $t_{CAO} - 1\,d$ to $t_{CAO} + 2\,d$ (Fig. 7j,l). Ridge amplification related to warm conveyor belt outflow associated with the primary cyclones as well as the width of the blocking ridge may explain the establishment of the blocking ridge in the western North Pacific (Steinfeld and Pfahl, 2019; Wenta et al., 2024).

https://doi.org/10.5194/egusphere-2026-2700
Preprint. Discussion started: 3 June 2026

Finally, the wave breaks cyclonically at $t_{CAO} + 2\,d$ (Fig. 7l, see PV anomaly in Fig. S3 in the supplement). The composites of small C_{BCAR} events are by far less impressive with a small ridge-trough couplet developing over eastern Asia shortly before the CAO events at $t_{CAO} - 2\,d$ (Fig. 7e). After the CAO event, the trough continues to propagate into North Pacific storm track without signs of additional downstream development (Fig. 7g,k).

Extending the theory by Takaya and Nakamura (2005a, b) with the principle of mutual intensification during baroclinic interaction, we propose that also the diabatically driven, cold-core surface anticyclone acts to amplify the upper-level ridge and thereby contributes to the evolution of the upper-level wave train. Following the PV perspective illustrated by Hoskins et al. (1985), near-surface diabatic cooling acts to reduce θ and yields a negative θ anomaly at the surface, that is associated with an anticyclonic circulation. Through the far-field effect, the anticyclonic circulation at the surface can then amplify the westward shifted, pre-existing negative PV anomaly at upper-levels (i.e., the ridge), just as in the case of cyclones baroclinically interacting with an upper-level trough. The vertical westward tilt of the surface anticyclone supports the hypothesis of baroclinic interaction taking place prior to large C_{BCAR} CAOs (Fig. 7b,d,f). Through the mechanism of baroclinic interaction, diabatic intensification of the surface anticyclone (as shown using the SLP tendency equation) may therefore also aid to amplify the upper-level wave. Although radiative cooling itself is a slow-process, the persistent Ural blocking ridge providing conditions for efficient and prolonged cooling may be able to initiate such an intensification cycle.

3.4 Impact on storm track activity and cyclone characteristics downstream

In section 3.1, section 3.2, and section 3.3 we showed that upstream near-surface radiative cooling contributes to enhanced low-level baroclinicity along the coast, a stronger Siberian high and a potentially amplified upper-levels Rossby wave featuring a deeper trough. In this final section, we now want to better elucidate the implications of these favorable conditions for the extratropical cyclones developing in the downstream storm track. For this purpose we compare the characteristics of the primary cyclones initiating the CAOs, as well as of the subsequent cyclones developing in the following days.

3.4.1 Characteristics of primary cyclones

Consistent with the anomalously high EGR prior to both CAOs types the primary cyclones achieve particularly high deepening rates (mean deepening rate of 1.4 Bergeron units for cyclones initiating small C_{BCAR} CAOs, and 1.54 Bergeron units for cyclones initiating large C_{BCAR} CAOs, see Fig. 8a). 79% and 69% of the primary cyclones initiating large or small C_{BCAR} CAOs qualify as bomb cyclones, respectively (Gyakum and Danielson, 2000). Estimating the climatological frequency of cyclones developing as bomb cyclones from the ratio of bomb cyclones to normal cyclones on random days (Table 1), this suggests an increase of the likelihood for explosive intensification of about 250% and 215% for cyclones associated with large and small C_{BCAR}, respectively. The high intensification rates culminate in deep cyclones with a mean depth of 963 hPa and 968 hPa for cyclones associated with large and small C_{BCAR} CAOs, respectively (Fig. 8b). Furthermore, the primary cyclones initiating large C_{BCAR} CAOs exhibit a slightly more northwards track, consistent with the large baroclinicity along the east Asian coast and the stagnating deep trough over the Japan Sea (Fig. S6 in the supplement, see Sect. 3.1 and Sect. 3.3). In summary, although primary cyclones associated with both types of CAOs exhibit anomalously high intensification rates and

https://doi.org/10.5194/egusphere-2026-2700
Preprint. Discussion started: 3 June 2026

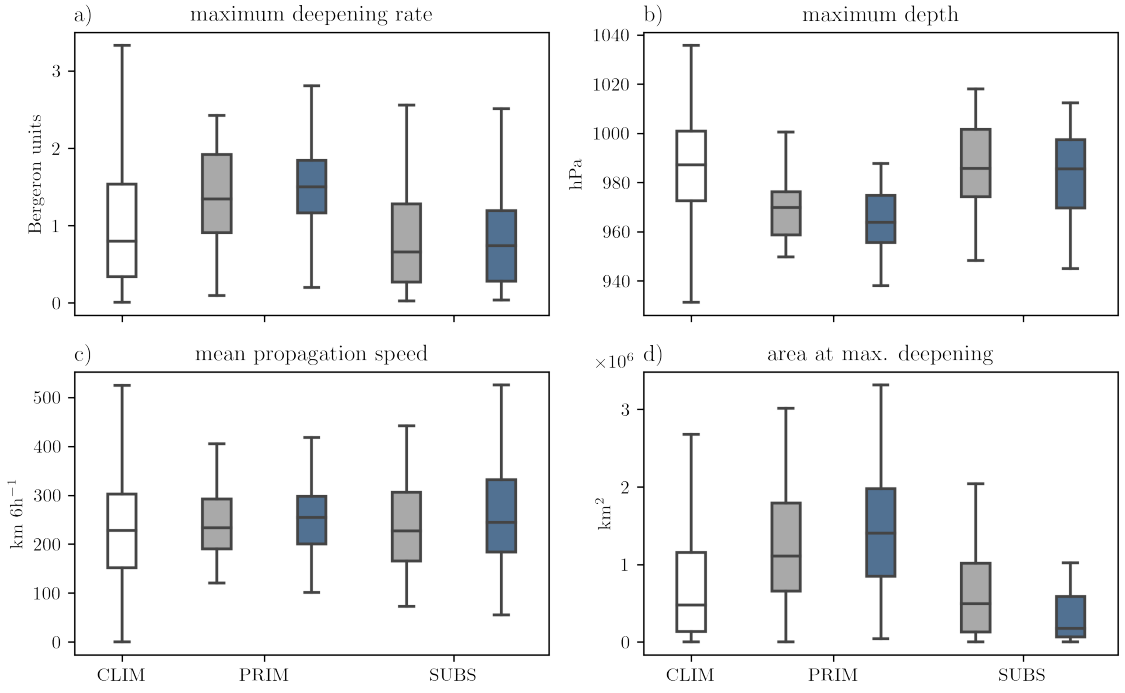

Figure 8. Characteristics of cyclones developing before (PRIM) and after (SUBS) CAOs featuring small (gray) and large (blue) BCAR contributions. We compare a) maximum intensification rates, and b) maximum depth, c) mean 6 h propagation speed, and d) area at the time of maximum deepening.

intensity, the ones initiating large C_{BCAR} CAOs consistently appear to be slightly more extreme and potentially more impactful for the coastal regions than the small C_{BCAR} (as a consequence of staying closer to the vicinity of Japan and Kamchatka).

3.4.2 Characteristics of subsequent cyclones

Comparing the number of cyclones developing in the days following CAOs, we find neither a difference in storm track activity between the 2 types of events nor with respect to climatology (Table 1). Although, we count more cyclones after CAOs featuring large BCAR contributions compared to periods after CAOs featuring small BCAR contributions (Table 1), significance testing with a Poisson rate test shows that such a difference is not significant (not shown). This is both the case for considering any intensifying cyclone or considering bomb cyclones only. Thus, we conclude that the storm track activity, at least in terms of cyclone number, is not affected by the occurrence of CAOs of either type and, therefore, also not affected by the diabatic cooling upstream. This is also consistent with Leeding et al. (2023), who found that the occurrence of North American cold spells did not alter the overall number of extratropical cyclones over the North Atlantic storm track, but rather affected their intensity and likelihood of explosive deepening. These findings suggest that cyclones are as likely to develop in the North

https://doi.org/10.5194/egusphere-2026-2700
Preprint. Discussion started: 3 June 2026

cyclone type	CAO type	1 - 2 d after CAO	1 - 3 d after CAO	1 - 4 d after CAO
all cyclones	small BCAR contr.	30	69	101
	large BCAR contr.	46	82	122
	random	38	80	102
bomb cyclones	small BCAR contr.	7	24	37
	large BCAR contr.	13	27	39
	random	12	26	40

Table 1. Number of intensifying cyclones during the given time window after CAOs featuring small or large BCAR contributions. Only cyclones with maximum intensification within a box from 130° - 180°E and 30° - 60°N are counted (see box in Fig. 2.

Pacific storm track after CAOs, although the depletion of baroclinicity near the coastline might imply changes in development regions consistent with the increased baroclinicity inside the storm track (see Sect. 3.1).

The characteristics of cyclones developing in the wake or at the edge of CAOs can differ substantially from the "primary" ones. The cyclones developing after large and small C_{BCAR} CAOs remain much smaller in size compared to the primary cyclones, and do not show the same impressive development in terms of maximum intensification rate or maximum intensity (Fig. 8a,b,d). In terms of propagation speed, the subsequent cyclones do not significantly differ from the primary cyclones nor climatology (Fig. 8c). In addition to the generally lower baroclinicity (see Sect. 3.1) cyclone-centered composites of QGω at the time of the cyclone's maximum intensification indicate that the forcing for ascent from upper levels is much weaker for the subsequent cyclones (Fig. 9). Differences in cyclone characteristics are especially pronounced between primary and subsequent cyclones associated with large C_{BCAR} CAOs. This is consistent with the environmental conditions in the storm track regions after large C_{BCAR} CAOs, characterized by cyclonic wave breaking at upper levels (therefore weaker forcing from upper-levels) and a less pronounced baroclinic zone, which – both combined together – do not support the growth of deep and large cyclones. As a result, precipitation is also focused much closer to the cyclone's center as opposed to the clearly recognizable frontal structures in the precipitation associated with the primary cyclones (Fig. 9). Thus, cyclones developing after CAOs remain unspectacular in comparison with primary cyclones and the climatology.

Given the shift in the location of the baroclinic zone as discussed in Sect. 3.1, it's also interesting to compare cyclogenesis regions. The majority of primary cyclones initiating large C_{BCAR} CAOs experience genesis in the vicinity of Japan or the Japan Sea with very few outliers closer to Kamchatka (Fig. S5 in the supplement). The genesis locations of their subsequent cyclones, however, are generally further westward and more scattered throughout the western North Pacific (Fig. S5 in the supplement). While a similar tendency can be observed before and after small C_{BCAR} CAOs, the patterns are not as pronounced (Fig. S4 in the supplement). Overall, this suggests that especially prior to large C_{BCAR} CAOs cyclogenesis is anchored closely at the coast, matching the high EGR values in the same location.

https://doi.org/10.5194/egusphere-2026-2700
Preprint. Discussion started: 3 June 2026

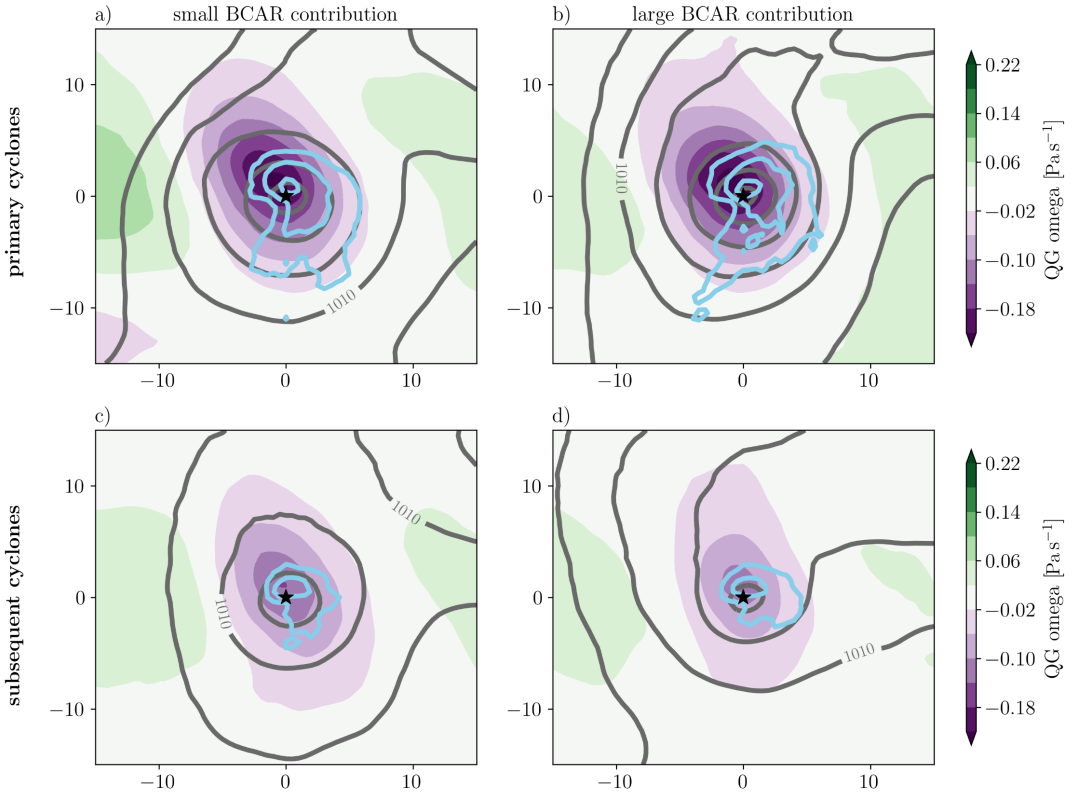

Figure 9. Cyclone-centered composites of the cyclones associated with the onset of the CAOs (a,b), and cyclones intensifying in the 1 to 3 days after CAOs (c,d) at the time of their maximum intensification. The cyclones are grouped based on their association with small (a,c) and large BCAR contribution CAOs (b,d). We show QGω at 600 hPa (shading), mean SLP (gray contours, every 5 hPa), and precipitation rates (blue contours, for 0.5, 1, and 2 mm h^{-1}).

4 Conclusions

4.1 Synthesis

Particularly strong CAOs in the Japan Sea and the Gulf Stream have previously been shown to be preceded by enhanced diabatic cooling over the upstream continent (Schnyder and Riboldi, 2026). In the current study, we exploit this connection to elucidate how upstream diabatic cooling can modulate the activity of the downstream North Pacific storm track. We do so by comparing CAOs featuring large and small C_{BCAR} (49 events each), indicative of stronger or weaker diabatic cooling over Siberia, resulting in stronger and weaker CAOs in the Japan Sea, respectively (Schnyder and Riboldi, 2026).

The CAOs in general, but especially the large C_{BCAR} type, are triggered by deep troughs and rapidly developing cyclones. Explosive cyclone development becomes more than twice as likely during CAO events (2.15 times with respect to climatology

https://doi.org/10.5194/egusphere-2026-2700
Preprint. Discussion started: 3 June 2026

Figure 10. Schematic representation of the two mechanisms how the upstream continent and the land sea contrast affect the North Pacific storm track on a synoptic timescale.

for small C_{BCAR} CAOs, and 2.5 times for large C_{BCAR} CAOs). We find that upstream diabatic cooling prior to large C_{BCAR} CAOs acts via two mechanisms to facilitate this environment conducive to explosively deepening cyclones (schematically illustrated in Fig. 10):

1. Diabatic cooling over land leads to accumulation of cold air over the continent, providing enhanced baroclinicity at the entrance of the storm tracks and promoting the growth of deep, explosively developing cyclones. After the intense CAOs initiated by these rapidly developing cyclones, the baroclinic zone is shifted eastward, away from the coast. At this time it is rather the cyclones within the storm track that modulate baroclinicity rather than the cooling upstream.

2. Diabatic cooling over land amplifies the surface anticyclone, contributing to a strong Siberian High. The surface anticyclone is coupled to an upper-level ridge, such that large-scale subsidence leads to conditions that allow for efficient radiative cooling, further promoting anticyclogenesis in the center and ahead of the anticyclone. Through the mechanism of baroclinic interaction, the diabatically intensified surface anticyclone is hypothesized to amplify the upper-level Rossby wave, resulting in a deep trough at the entrance of the storm track and a cyclonic wave breaking in the days after.

The two mechanisms combined lead to an oscillation of the North Pacific storm track between two states. During periods of enhanced cooling over the land surface, baroclinicity gradually builds up along the coastline, as cold air accumulates over the continent (Fig. 10a). At the same time, wave trains propagating over Siberia are amplified leading to a deep trough entering the storm track (Fig. 10a). On account of the high baroclinicity and strong forcing for ascent due to the deep trough, the likelihood for explosive cyclone development is substantially increased. These cyclones, initiating intense CAOs, achieve particularly low depth and advect the cold continental air into the storm tracks, thus shifting the baroclinic zone away from the coast (Fig. 10b). During this time, the baroclinicity is modulated rather by cyclones in the storm tracks than by cooling over the upstream continent. Although cyclones may still develop on the new baroclinic zone further inside the storm track, baroclinicity is not as high and the forcing from the upper levels is weaker than before the CAO. As a result, the cyclones do not achieve the same

https://doi.org/10.5194/egusphere-2026-2700
Preprint. Discussion started: 3 June 2026

intensities and remain smaller in size compared to the primary cyclones. Eventually, continuous cooling over the upstream continent and strong fluxes associated with the CAO gradually replenish the baroclinicity at the entrance of the storm track, shifting the zone of baroclinicity closer to the coast line again.

4.2 Discussion

Our results agree well with the nonlinear oscillator model proposed by Novak et al. (2015), which states that large baroclinicity at the entrance of the storm tracks is consumed by developing cyclones, that shift the storm tracks location. The cyclonic wave breaking, which follows the rapid development of the cyclone, is associated with an equatorward shift of the jet. While baroclinicity is still available after the CAOs, EGR along the coastline are generally lower compared to before the CAO's occurrence and the location of largest EGR is shifted away from the continent. This results in different regions actively contributing to the storm tracks (Schemm et al., 2021) and in smaller, less rapidly developing cyclones in comparison to the primary cyclones. During this time period, the cyclones developing in the storm tracks are the responsible of maintaining baroclinicity thereby (Papritz and Spengler, 2015; Marcheggiani and Spengler, 2023), while air-sea fluxes in the CAO region slowly build up baroclinicity near the coastline (Marcheggiani and Spengler, 2025). As soon as a new upper-level wave approaches Siberia, enhanced diabatic cooling over the upstream continent contributes again to the build-up of large baroclinicity along the coast line, and the oscillation begins again. Thus, by exploring the role of upstream diabatic cooling in addition to the known processes occurring within the storm tracks, this study provides a mechanistic perspective on the storm tracks' oscillating behavior.

The amplification of the upper-level wave train through baroclinic interaction of a diabatically enhanced surface anticyclone plays a crucial role for this development. Using the SLP tendency equation, we were able to show that diabatic cooling significantly contributes to the surface anticyclone's intensification with an average intensification rate of about 3 hPa ($6\,h^{-1}$). While there is evidence for the occurrence of baroclinic interaction (e.g., the vertical tilt between the surface anticyclone and the upper-level ridge prior to large C_{BCAR} CAOs, as in Fig. 7 of Takaya and Nakamura, 2005b), it is yet to be shown that the far-field effect of the surface anticyclonic circulation can effectively reach the upper-level ridge, and is able to amplify the upper-level wave. An obstacle here could be constituted by the rather high static stability of the cold air mass limiting the Rossby penetration depth; this problem, however, might be alleviated by the relatively low tropopause height usually found at high latitudes during winter. Idealized simulations featuring an upper-level wave train and a local cooling source at the surface could provide more precise insights into the dynamics of this peculiar interaction.

Finally, we believe that this study can shed new light on land-sea contrast, a climatological feature classically regarded as a fundamental driver of storm track activity (e.g., Brayshaw et al., 2009). The results of the current study imply that land-sea contrast is not only a potential modulator of downstream weather systems, but is in itself modulated by weather systems upstream of the coastline, such as the Siberian High, upstream Rossby wave trains or atmospheric blocking. The fact that the net radiative energy loss at the surface can vary with time provides a physical mechanism that can explain variations in background baroclinicity at the weekly to sub-seasonal scale: periods of extended Ural blocking, for instance, would likely correspond to enhanced land-sea contrast at the entrance of the North Pacific storm track. Treating land-sea contrast as a non-stationary forcing can provide a more realistic representation of the processes "replenishing" baroclinicity at the entrance of

https://doi.org/10.5194/egusphere-2026-2700
Preprint. Discussion started: 3 June 2026

the storm track, explaining at the same time the absence of a clear periodicity in the observations of EGR and meridional eddy heat flux discussed in the conclusions of Ambaum and Novak (2014). As the radiative processes generating cold air over the continent are relatively slow, their explicit consideration might also be exploited to constrain storm track activity, with potential gains in medium-range predictability, or to enhance physical understanding of how the extratropical circulation will change in future, warmer climates.

Code and data availability. The ERA5 reanalyses (Hersbach et al., 2020) can be obtained from the Copernicus Climate Change Service, Climate Data Store (https://doi.org/10.24381/cds.adbb2d4). The ERA5 climatology of QG-forcing for ascent used in this study are available from the authors upon request.

Author contributions. FS ideated and conducted the analysis behind the study, and wrote the manuscript. JR supported FS in the analysis and interpretation of the results, and participated in the writing process with feedback and editing.

Competing interests. We declare that no competing interests are present.

Acknowledgements. We would like to express our deep appreciation to Michael Sprenger (ETH Zürich) for providing EGR, QGω and cyclone track data, as well as his great support in our pursuit of anticyclone tracking. We are also very grateful to Svenja Christ and Ting-Chen Chen (Karlsruhe Institut für Technologie, KIT) for providing us with the scripts to compute the SLP tendency equation on ERA5 data, and Lukas Papritz and Heini Wernli (both ETH) for the insightful discussions on the results of this study. The authors acknowledge funding from the Swiss National Science Foundation (SNSF) via grant PZ00P2_209135.

https://doi.org/10.5194/egusphere-2026-2700
Preprint. Discussion started: 3 June 2026

References

Ambaum, M. H. P. and Novak, L.: A nonlinear oscillator describing storm track variability, Q. J. Roy. Meteorol. Soc., 140, 2680–2684, https://doi.org/https://doi.org/10.1002/qj.2352, 2014.

Besson, P., Fischer, L. J., Schemm, S., and Sprenger, M.: A global analysis of the dry-dynamic forcing during cyclone growth and propagation, Weather Clim. Dynam., 2, 991–1009, https://doi.org/10.5194/wcd-2-991-2021, 2021.

Bosart, L. F.: The Presidents' Day snowstorm of 18–19 February 1979: A subsynoptic-scale event, Mon. Weather Rev., 109, 1542–1566, https://doi.org/10.1175/1520-0493(1981)109<1542:TPDSOF>2.0.CO;2, doi: 10.1175/1520-0493(1981)109<1542:TPDSOF>2.0.CO;2, 1981.

Brayshaw, D. J., Hoskins, B., and Blackburn, M.: The basic ingredients of the North Atlantic storm track. Part I: land–sea contrast and orography, J. Atmos. Sci., 66, 2539 – 2558, https://doi.org/10.1175/2009JAS3078.1, 2009.

Christ, S., Quinting, J., and Pinto, J. G.: Characteristics of diabatically influenced cyclones with high wind damage potential in Europe, Q. J. Roy. Meteorol. Soc., p. e70083, https://doi.org/https://doi.org/10.1002/qj.70083, 2025.

Curry, J.: On the formation of continental polar air, J. Atmos. Sci., 40, 2278–2292, https://doi.org/10.1175/1520-0469(1983)040<2278:OTFOCP>2.0.CO;2, doi: 10.1175/1520-0469(1983)040<2278:OTFOCP>2.0.CO;2, 1983.

Curry, J.: The contribution of radiative cooling to the formation of cold-core anticyclones, J. Atmos. Sci., 44, 2575–2592, https://doi.org/10.1175/1520-0469(1987)0442.0.CO;2, 1987.

Davies, H. C.: The Quasigeostrophic Omega Equation: reappraisal, refinements, and relevance, Mon. Weather Rev., 143, 3 – 25, https://doi.org/10.1175/MWR-D-14-00098.1, 2015.

Ding, Y. and Krishnamurti, T. N.: Heat budget of the Siberian High and the winter monsoon, Mon. Weather Rev., 115, 2428 – 2449, https://doi.org/10.1175/1520-0493(1987)115<2428:HBOTSH>2.0.CO;2, 1987.

Fink, A. H., Pohle, S., Pinto, J. G., and Knippertz, P.: Diagnosing the influence of diabatic processes on the explosive deepening of extratropical cyclones, Geophys. Res. Lett., 39, https://doi.org/https://doi.org/10.1029/2012GL051025, 2012.

Gyakum, J. R. and Danielson, R. E.: Analysis of meteorological precursors to ordinary and explosive cyclogenesis in the Western North Pacific, Mon. Weather Rev., 128, 851–863, https://doi.org/10.1175/1520-0493(2000)128<0851:AOMPTO>2.0.CO;2, doi: 10.1175/1520-0493(2000)128<0851:AOMPTO>2.0.CO;2, 2000.

Hersbach, H., Bell, B., Berrisford, P., Hirahara, S., Horányi, A., Muñoz-Sabater, J., Nicolas, J., Peubey, C., Radu, R., Schepers, D., Simmons, A., Soci, C., Abdalla, S., Abellan, X., Balsamo, G., Bechtold, P., Biavati, G., Bidlot, J., Bonavita, M., Chiara, G., Dahlgren, P., Dee, D., Diamantakis, M., Dragani, R., Flemming, J., Forbes, R., Fuentes, M., Geer, A., Haimberger, L., Healy, S., Hogan, R. J., Hólm, E., Janisková, M., Keeley, S., Laloyaux, P., Lopez, P., Lupu, C., Radnoti, G., Rosnay, P., Rozum, I., Vamborg, F., Villaume, S., and Thépaut, J.: The ERA5 global reanalysis, Q. J. R. Meteor. Soc., 146, 1999–2049, https://doi.org/10.1002/qj.3803, doi: 10.1002/qj.3803, 2020.

Hoskins, B. J. and Hodges, K. I.: New perspectives on the Northern Hemisphere winter storm tracks, J. Atmos. Sci., 59, 1041–1061, https://doi.org/10.1175/1520-0469(2002)059<1041:NPOTNH>2.0.CO;2, doi: 10.1175/1520-0469(2002)059<1041:NPOTNH>2.0.CO;2, 2002.

Hoskins, B. J., Mcintyre, M. E., and Robertson, A. W.: On the use and significance of isentropic potential vorticity maps, Q. J. R. Meteor. Soc., 111, 877–946, doi: 10.1002/qj.49711147002, 1985.

https://doi.org/10.5194/egusphere-2026-2700
Preprint. Discussion started: 3 June 2026

Kuo, Y.-H., Reed, R. J., and Low-Nam, S.: Effects of surface energy fluxes during the early development and rapid intensification stages of seven explosive cyclones in the western Atlantic, Mon. Weather Rev., 119, 457–476, doi: 10.1175/1520-0493(1991)119<0457:EOSEFD>2.0.CO;2, 1991.

Leeding, R., Riboldi, J., and Messori, G.: Modulation of North Atlantic extratropical cyclones and extreme weather in Europe during North American cold spells, Weather Clim. Extreme, 42, 100 629, https://doi.org/https://doi.org/10.1016/j.wace.2023.100629, 2023.

Marcheggiani, A. and Spengler, T.: Diabatic effects on the evolution of storm tracks, Weather Clim. Dyn., 4, 927–942, https://doi.org/10.5194/wcd-4-927-2023, 2023.

Marcheggiani, A. and Spengler, T.: Cold air outbreaks drive near-surface baroclinicity variability over storm track entrance regions in the Northern Hemisphere, Weather Clim. Dyn., 6, 1479–1489, https://doi.org/10.5194/wcd-6-1479-2025, 2025.

Marcheggiani, A., Dacre, H., Spensberger, C., and Spengler, T.: Weather features drive free-tropospheric baroclinicity variability in the North Atlantic storm track, Q. J. Roy. Meteorol. Soc., 151, e5061, https://doi.org/https://doi.org/10.1002/qj.5061, 2025.

Namias, J.: The index cycle and its role in the general circulation, J. Atmos. Sci., 7, 130 – 139, https://doi.org/10.1175/1520-0469(1950)007<0130:TICAIR>2.0.CO;2, 1950.

Novak, L., Ambaum, M. H. P., and Tailleux, R.: The Life Cycle of the North Atlantic Storm Track, J. Atmos. Sci., 72, 821 – 833, https://doi.org/10.1175/JAS-D-14-0082.1, 2015.

Owen, L. E., Catto, J. L., Stephenson, D. B., and Dunstone, N. J.: Compound precipitation and wind extremes over Europe and their relationship to extratropical cyclones, Weather Clim. Extrem., 33, 100 342, https://doi.org/https://doi.org/10.1016/j.wace.2021.100342, 2021.

Papritz, L. and Spengler, T.: Analysis of the slope of isentropic surfaces and its tendencies over the North Atlantic, Q. J. Roy. Meteor. Soc., 141, 3226–3238, https://doi.org/10.1002/qj.2605, doi: 10.1002/qj.2605, 2015.

Papritz, L., Pfahl, S., Sodemann, H., and Wernli, H.: A climatology of cold air outbreaks and their impact on air-sea heat fluxes in the high-latitude South Pacific, J. Climate, 28, 342–364, https://doi.org/10.1175/JCLI-D-14-00482.1, doi: 10.1175/JCLI-D-14-00482.1, 2015.

Pfahl, S. and Wernli, H.: Quantifying the relevance of cyclones for precipitation extremes, J. Climate, 25, 6770–6780, https://doi.org/10.1175/JCLI-D-11-00705.1, 2012.

Pinto, J. G., Gómara, I., Masato, G., Dacre, H. F., Woollings, T., and Caballero, R.: Large-scale dynamics associated with clustering of extratropical cyclones affecting Western Europe, J. Geophys. Res., 119, 13–704, https://doi.org/10.1002/2014JD022305, 2014.

Portal, A., Pasquero, C., D'Andrea, F., Davini, P., Hamouda, M. E., and Rivière, G.: Influence of reduced winter land-sea contrast on the midlatitude atmospheric circulation, J. Climate, 35, 6237–6251, https://doi.org/10.1175/JCLI-D-21, doi: 10.1175/JCLI-D-21, 2022.

Portal, A., D'Andrea, F., Davini, P., Hamouda, M. E., and Pasquero, C.: Atmospheric response to cold wintertime Tibetan Plateau conditions over eastern Asia in climate models, Weather Clim. Dyn., 4, 809–822, https://doi.org/10.5194/wcd-4-809-2023, doi: 10.5194/wcd-4-809-2023, 2023.

Qian, Q., Zhong, W., Yao, Y., and Zhang, D.: Influence of the Thermal Structure on the Intensification of the Extreme Arctic Cyclone in August 2016, J. Geophys. Res. Atmos., 128, e2023JD038 638, https://doi.org/https://doi.org/10.1029/2023JD038638, e2023JD038638 2023JD038638, 2023.

Schemm, S., Wernli, H., and Binder, H.: The storm-track suppression over the western North Pacific from a cyclone life-cycle perspective, Weather Clim. Dyn., 2, 55–69, https://doi.org/10.5194/wcd-2-55-2021, 2021.

https://doi.org/10.5194/egusphere-2026-2700
Preprint. Discussion started: 3 June 2026

Schnyder, F. and Riboldi, J.: Linking upstream cold, continental air to the intensity of marine cold-air outbreaks along the western boundary currents of the North Pacific and North Atlantic: A lagrangian analysis, J. Climate, 39, 2243—-2262, https://doi.org/10.1175/JCLI-D-25-0336.1, 2026.

Shoji, T., Kanno, Y., Iwasaki, T., and Takaya, K.: An isentropic analysis of the temporal evolution of East Asian cold air outbreaks, J. Climate, 27, 9337–9348, https://doi.org/10.1175/JCLI-D-14-00307.1, doi: 10.1175/JCLI-D-14-00307.1, 2014.

Sprenger, M. and Wernli, H.: The LAGRANTO Lagrangian analysis tool - Version 2.0, Geosci. Model Dev., 8, 2569–2586, https://doi.org/10.5194/gmd-8-2569-2015, doi: 10.5194/gmd-8-2569-2015, 2015.

Sprenger, M., Fragkoulidis, G., Binder, H., Croci-Maspoli, M., Graf, P., Grams, C. M., Knippertz, P., Madonna, E., Schemm, S., Škerlak, B., and Wernli, H.: global climatologies of eulerian and lagrangian flow features based on ERA-Interim, B. Am. Meteorol. Soc., 98, 1739–1748, https://doi.org/10.1175/BAMS-D-15-00299.1, doi:10.1175/BAMS-D-15-00299.1, 2017.

Steinfeld, D. and Pfahl, S.: The role of latent heating in atmospheric blocking dynamics: a global climatology, Clim. Dyn., 53, 6159–6180, https://doi.org/10.1007/s00382-019-04919-6, doi: 10.1007/s00382-019-04919-6, 2019.

Takaya, K. and Nakamura, H.: Geographical dependence of upper-level blocking formation associated with intraseasonal amplification of the Siberian High, J. Atmos. Sci., 62, 4441–4449, doi: 10.1175/JAS3628.1, 2005a.

Takaya, K. and Nakamura, H.: Mechanisms of intraseasonal amplification of the cold Siberian High, J. Atmos. Sci., 62, 4423 – 4440, https://doi.org/10.1175/JAS3629.1, 2005b.

Vannière, B., Czaja, A., Dacre, H., and Woollings, T.: A "cold path" for the gulf stream-troposphere connection, J. Climate, 30, 1363–1379, https://doi.org/10.1175/JCLI-D-15-0749.1, doi: 10.1175/JCLI-D-15-0749.1, 2017.

Weijenborg, C. and Spengler, T.: Detection and global climatology of two types of spatio-temporal clustering of extratropical cyclones, Weather Clim. Dyn., 7, 475–488, https://doi.org/10.5194/wcd-7-475-2026, 2026.

Wenta, M., Grams, C. M., Papritz, L., and Federer, M.: Linking Gulf Stream air–sea interactions to the exceptional blocking episode in February 2019: a Lagrangian perspective, Weather Clim. Dyn., 5, 181–209, https://doi.org/10.5194/wcd-5-181-2024, doi: 10.5194/wcd-5-181-2024, 2024.

Wernli, H. and Schwierz, C.: Surface cyclones in the ERA-40 dataset (1958-2001). Part I: novel identification method and global climatology, J. Atmos. Sci., 63, 2486–2507, doi: 10.1175/JAS3766.1, 2006.

Wexler, H.: Formation of polar anticyclones, Mon. Weather Rev., 65, 229—-236, https://doi.org/10.1175/1520-0493(1937)652.0.CO;2, 1937.

Wexler, H.: Anticyclones, pp. 621–629, American Meteorological Society, Boston, MA, https://doi.org/10.1007/978-1-940033-70-9_50, 1951.

Wilks, D. S.: The stippling shows statistically significant grid points": How research results are routinely overstated and Overinterpreted, and What to Do about It, B. Am. Meteorol. Soc., 97, 2263 – 2273, https://doi.org/10.1175/BAMS-D-15-00267.1, 2016.